Analytical Methods

ROYAL SOCIETY OF CHEMISTRY

PAPER

View Article Online
View Journal

Cite this: DOI: 10.1039/d0ay00921k

Electrochemical chiral amino acid biosensor based on dopamine-localized gold nanoparticles @ left-handed spiral chiral carbon nanotubes

Haijun Lu,† Zimeng Wang,† Xinyu Fan, Haiyang Wang, Qi Zhang, Mingxuan Fu, Guyang Ning, Yufan Zhang * and Huan Wang *

The high electrocatalytic performance plays a decisive role in the efficient electrochemical sensing of electrocatalysts. A spiral chiral carbon tube (HLCNT) loaded with gold nanoparticles (AuNPs) was prepared by electrochemical methods. Dopamine was first electropolymerized on the surface of the HLCNT, and then it acted as a localizer to uniformly load the AuNPs onto the surface of the HLCNT. The dopamine-localized gold nanoparticles @ left-handed spiral chiral carbon nanotubes (HLCNT-AuNPs-2) material combined the chiral structure of chiral carbon nanotubes and the high conductivity of AuNPs. The HLCNT-AuNPs-2 realized the qualitative and quantitative detection of tyrosine (Tyr) and tryptophan (Trp) isomers by their different oxidation potentials and current signals. Through quantitative detection, the analytical results showed that the detection limit of L-Trp was calculated to be 5.31 μM, and the detection limit of L-Tyr was 9.04 μM. More importantly, the material realized the real sample detection of amino acids, which is of great significance for the practical detection of amino acid isomers in medicine and biology.

Received 7th May 2020
Accepted 6th July 2020

DOI: 10.1039/d0ay00921k

rsc.li/methods

Introduction

Chiral phenomena are widely found in nature and have important significance in life sciences, materials science, and pharmaceuticals.[1,2] Chiral phenomena present a rich and diverse form of expression in both nature and life. In daily life, the chiral appearance can be seen everywhere, such as DNA. In addition, chirality in amino acid plays an important role and participates in numerous physiological processes in living systems.[3] Tyrosine (Tyr) plays an important role in regulating various biological signalling molecules. Tryptophan (Trp) plays a vital physiological role in biological systems,[4–6] and is related to human metabolism and physiological functions.[7,8] The concentration of Trp in human blood is very important because it may be behind the causes of many diseases.[9] The chiral nature of amino acids is different, and its roles in organisms are also very different. For example, L-Tyr is an essential amino acid that can treat depression and bipolar disorder. However, D-Tyr is a non-essential amino acid that can be used to synthesize pharmaceutical materials. Therefore, the chirality recognition of amino acids plays a crucial role in biomedical research, the pharmaceutical industry and clinical applications.[10,11]

At present, the chiral recognition methods are mainly divided into three major categories: chromatography, spectroscopy and electrochemical methods. Spectroscopy and chromatography have many advantages in chiral recognition and separation, but they are also have some limitations, such as high equipment costs, complex pretreatment steps and long detection times. Electrochemical methods have the advantages of low cost, low pollution and rapid detection, and have great development prospects.[12] Haldorai *et al.* studied a tin oxide nanoparticle chiral sensor and the recognition of tryptophan by an electrochemical method.[13] Tao *et al.* developed an electrochemical chiral sensor based on alpha-cyclodextrin (alpha-CD) to identify the Tyr enantiomer.[11] Zeng *et al.* reported an electrochemical sensor by polymerizing organic matter on a glassy carbon electrode for identifying glutamate isomers.[14] Kingsford *et al.* modified the electrode by using carbon black/poly-L-cysteine and then used this for electrochemical identification of the tryptophan enantiomer.[15] In these works discussed above, most used nanomaterials as chiral catalysts to achieve the chiral biosensing, but still their electrocatalytic performance needs to be further improved. In addition, if the electrocatalytic performance is to be improved, chiral carbon nanomaterials would be a better choice. Therefore, we aimed to study the chiral recognition interface based on chiral carbon nanomaterials as a chiral biosensor.

Key Laboratory of Analytical Science and Technology of Hebei Province, Key Laboratory of Medicinal Chemistry and Molecular Diagnosis, Ministry of Education, College of Chemistry and Environmental Science, Hebei University, Baoding 071002, Hebei Province, P. R. China. E-mail: zwhsjzl@163.com; Fax: +86 0312 5079403; Tel: +86 0312 5079403

† Haijun Lu and Zimeng Wang are contributed equally to this article.

Among many new nanomaterials, carbon nanomaterials have attracted great interest from researchers due to their low density, excellent electrical and electrocatalytic properties. At present, electrochemical biosensing research based on carbon nanomaterials is becoming a research hotspot, and has attracted extensive attention in scientific and commercial circles. Carbon nanotubes[16,17] have been widely used in the field of electrochemical biosensing as a modified electrode material, and have shown superior electrocatalytic performance over conventional carbon materials.[18] For chiral biosensing catalysts, lots of works are based on the surface functionalization of carbon nanomaterials to achieve chiral biosensing properties.[16,19,20] For new carbon nanomaterials, the development and preparation of materials with chiral topography and nanostructures can help achieve higher chirality biosensing performance. Therefore, the study of chiral carbon nanomaterials is particularly important. In addition, in the preparation of high-sensitivity electrochemical chiral sensors, many studies use a single strategy to identify and quantify amino acid enantiomers, while strategies for the quantitative detection of amino acid enantiomers by differences in the current and potential signals are rarely used. Therefore, it would be significant to develop a simple strategy for identifying and quantifying sensitive chiral electrochemical sensors for amino acid enantiomers based on differences in the potential and current.

For these reasons, a highly efficient electrochemical chiral biosensing system based on left-handed helix carbon nanotubes @ gold nanoparticles (HLCNT-AuNPs-2) composites was synthesized. On the surface of the left-handed carbon nanotubes, PDA was polymerized on its surface by electropolymerization. Dopamine has self-polymerizing oxidation properties,[21] and is attractive to researchers due to its great practicality and simplicity. It can act as a localizer to uniformly load the gold nanoparticles (AuNPs) onto the surface of the HLCNT, to make the AuNPs highly dispersed on the surface of HLCNT. AuNPs have high catalytic activity and play an important role in promoting charge transfer between electrodes and species.[22–24] In this work, an HLCNT/AuNPs composite was successfully prepared, and then successfully used to achieve the quantitative detection of a Tyr and Trp mixed solution by using the potential difference and current difference signal. It enabled the efficient electrochemical biosensing of amino acid isomers in this nanocomposite, which demonstrated the method's utility for constructing a highly sensitive electrochemical chiral biosensor.

Experimental

Reagents and apparatus

L,D-Tryptophan (Trp), L,D-tyrosine (Tyr), L-glutamic acid, myristoyl chloride, pyrrole, and *N*,*N*-dimethylformamide (DMF) were purchased from Aladdin Industrial Corporation (Shanghai, China). KNO_3, $HAuCl_4$, and dopamine hydrochloride (DA) were purchased from Shanghai Chemical Industry Park (Shanghai, China). Phosphate buffer solution (PBS, pH 7.4), which consisted of NaH_2PO_4, Na_2HPO_4, and Na_3PO_4, was used as the supporting electrolyte. All chemicals were of analytical grade.

Electrochemical detection was performed on an Autolab electrochemical workstation (PGSTAT-302N, Metrohm Switzerland), with a traditional three-electrode system used, where a platinum electrode was used as the counter electrode, a Ag/AgCl electrode was used as the reference electrode, and a modified glassy carbon electrode (GCE, 3 mm diameter) served as the working electrode.

Scanning electron microscopy (SEM) images were obtained using a Philips XL-30 ESEM system. Transmission electron microscopy (TEM) images of the fabricated samples were obtained with a JEM-2100F transmission electron microscope (JEOL, Japan) operating at 200 kV. X-ray photoelectron spectroscopy (XPS) was performed on a Thermo ESCA LAB Spectrometer (USA). Nitrogen adsorption–desorption isotherms were determined on an ASAP 2020 system.

Preparation of HLCNT samples

1. **Preparation of C_{18}-L-Glu.** First, the amino acid surfactant C_{18}-L-Glu was prepared according to the following steps:[25] 35.5 g L-glutamic acid was added into a mixed solution of deionized water (140 mL), acetone (120 mL), and 0.480 mol NaOH (19.2 g). It was thoroughly stirred at 30 °C, then 60.5 g of myristoyl chloride was added dropwise to the mixed solution under ice-cold conditions, and 20 mL of NaOH (0.2 M) was added while maintaining the pH at 12. The reaction was continued for 1 h and then acidified to pH 1 with 12 M HCl, then washed to obtain the surfactant C_{18}-L-Glu. Finally, the resulting sample was centrifuged with deionized water and petroleum ether and lyophilized at −60 °C.

2. **Preparation of the HLCNT sample.** According to the method reported,[18] C_{18}-L-Glu (0.06 mmol) was dissolved in methanol (12.9 mL); then pyrrole (2.4 mmol) and deionized water (60 mL) were added and the mixture was fully stirred for 10 min. An additional 2.0 M of precooled aqueous ammonium persulfate solution was added to the mixture, and the mixture was continuously stirred for 30 min. The chiral polypyrrole nanotube was obtained by filtration and washed with double distilled water, and then dried in vacuum at 40 °C. Finally, the enantiopure HLCNT sample was obtained by carbonizing chiral polypyrrole at 900 °C under an N_2 atmosphere.

Preparation of the modified electrode

GCE was polished before each experiment with 0.05 μm alumina powder and rinsed thoroughly with doubly distilled water. Then the cleaned electrode was dried with high-purity nitrogen for the next modification. To prepare the modified electrode, 2 mg of the as-prepared HLCNT sample was dispersed into 1 mL dimethyl formamide (DMF) to give a homogeneous suspension (2 mg mL^{-1}) upon bath sonication. The HLCNT/GCE was prepared by casting 10 μL of the HLCNT suspension on the surface of GCE and the solvent was allowed to dry under an infrared lamp.

1. **Preparation of HLCNT-DA/GCE.** HLCNT-DA/GCE was obtained by placing HLCNT/GCE in 2 mM DA solution and

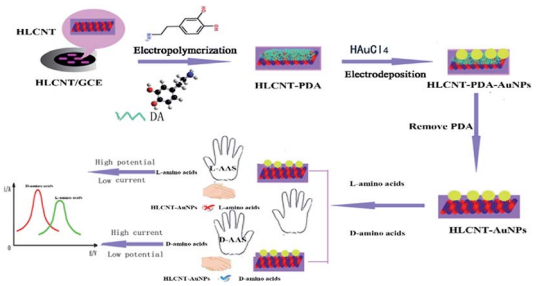

Scheme 1 Schematic of the construction of the chiral electrode interface and the mechanism for the recognition of amino acid isomers.

subjected to cyclic voltammetry for 20 cycles at a potential of −0.7∼0.7 V at a rate of 100 mV s^{-1}.

2. Preparation of HLCNT-DA-AuNPs/GCE. The HLCNT-DA/GCE electrode was placed in a 0.1 M KNO_3–0.2 g L^{-1} $HAuCl_4$ solution, then scanned by a time current method at a potential of −0.2 V for 60 s to obtain HLCNT-DA-AuNPs/GCE.

3. Preparation of HLCNT-AuNPs-1/GCE. HLCNT-AuNPs-1/GCE was prepared by placing HLCNT/GCE in a 0.1 M KNO_3–0.2 g L^{-1} $HAuCl_4$ solution, then scanned by a time current method for 60 s at a potential of −0.2 V.

4. Preparation of the HLCNT-AuNPs-2 material. The HLCNT-DA-AuNPs/GCE electrode was placed in 0.1 M KOH for 2 h, then rinsed off after washing to get HLCNT-AuNPs-2/GCE.

Scheme 1 shows the preparation process of the HLCNT-AuNPs-2/GCE.

Results and discussion

Characterization of HLCNT-AuNPs-2

The SEM and TEM characterization of HLCNT, HLCNT-AuNPs-1 and HLCNT-AuNPs-2 materials were performed.

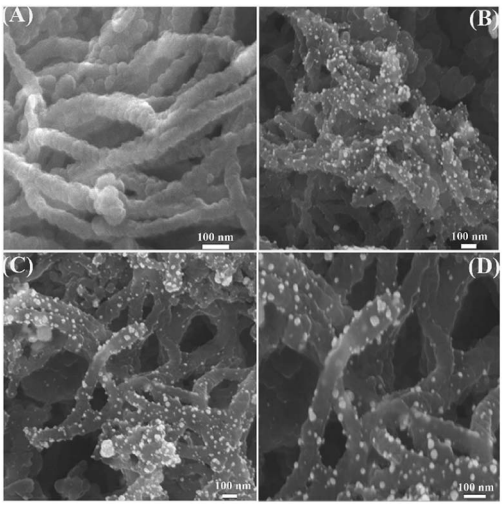

Fig. 1 SEM images of the different materials: (A) HLCNT, (B) HLCNT-AuNPs-1; (C) and (D) HLCNT-AuNPs-2.

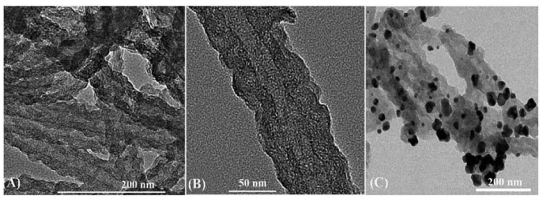

Fig. 2 TEM images of (A) and (B) HLCNT, (C) HLCNT-AuNPs-2.

As can be seen from the Fig. 1 A, we can see that HLCNT is a long tubular surface with a rough surface and a double helix chiral structure, where the double-helical morphology of the nanotubes was still well-maintained, even after carbonization at high temperatures (*e.g.* 900 °C);[18] thus displaying its high ability to memorize the original morphology. It is apparent from Fig. 1B that AuNPs are loaded on HLCNT in the HLCNT-AuNPs-1, while the AuNPs in Fig. 1C, D and 2C are more evenly dispersed in HLCNT-AuNPs-2 compared with HLCNT-AuNPs-1, this is due to DA having the function of connecting with trivalent gold ions, which can highly disperse the gold nanoparticles on the surface of HLCNT. Furthermore, the TEM images of HLCNT show that the internal structure of HLCNT is hollow (Fig. 2A and B) and the surface of HLCNT is folded, which may be the characteristic structure of graphitized carbon. At the same time, it further illustrates that HLCNT has a double helix structure. This structure is beneficial to accelerate mass transfer and electron transfer.

Fig. 3 illustrates the nitrogen adsorption–desorption isotherm and the related pore-size distribution of the HCNT material. This indicates that the isotherm of HLCNT was

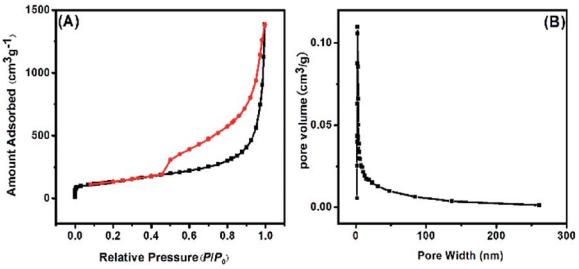

Fig. 3 (A) Nitrogen adsorption–desorption isotherms of HLCNT; (B) pore-size distribution curve of HLCNT.

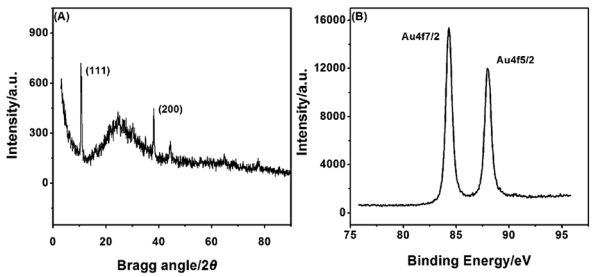

Fig. 4 (A) XRD spectrum of HLCNT-AuNPs-2, (B) high-resolution Au 4f XPS spectrum of HLCNT-AuNPs-2.

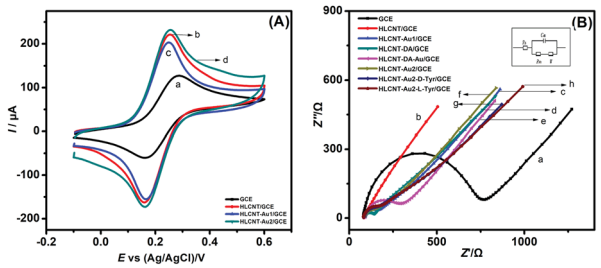

Fig. 5 (A) Cyclic voltammograms (CVs) of GCE (a), HLCNT/GCE (b), HCNT-AuNPs-1/GCE (c) and HCNT-AuNPs-2/GCE (d) in 5 mM $[Fe(CN)_6]^{3-/4-}$ (1 : 1) in 0.1 M KCl. Scan rate: 50 mV s^{-1}; (B) EIS of GCE (a), HLCNT/GCE (b), HLCNT-AuNPs-1/GCE (c), HLCNT@DA/GCE (d), HLCNT@DA-Au/GCE (e), HLCNT-AuNPs-2/GCE (f), HLCNT-AuNPs-2-D-Tyr/GCE (g),HLCNT-AuNPs-2-L-Tyr/GCE (h) in the 1 : 1 solution of 5 mM $Fe(CN)_6^{3-/4-}$ and 0.1 M KCl. The frequency range is from 1.00 Hz to 100 KHz. Inset: Randles equivalent circuit.

a typical type IV, with an H1 type hysteresis line, indicating that HLCNT is a microporous structure. The Brunauer–Emmett–Teller (BET) specific surface area was 479.33 m^2 g^{-1}. The HLCNT also had a narrow pore-size distribution with an intensity peak at 9.7866 nm, thus displaying a uniform microporous feature.

In the XRD diagram (Fig. 4A), two diffraction peaks could be noted, appearing at 10.75° and 38.14°, which correspond to the (111) and (200) diffractions of the Au standard peak, respectively. Therefore, it was proved that the phase of the AuNPs structure was face-centred cubic (fcc). As shown in Fig. 4B, the XPS spectra exhibited two peaks corresponding to Au $4f_{7/2}$ and Au $4f_{5/2}$, displaying that the AuNPs had been successfully loaded onto the HLCNT-AuNPs-2. All the characterizations proved that HLCNT-AuNPs-2 was successfully synthesized.

Electrochemical detection

During the manufacture of the HLCNT-AuNPs-2, the electrochemical properties of the electrode were gradually characterized by CV and EIS, and the results are shown in Fig. 5A and B. As shown in Fig. 5A, the cyclic voltammograms of different electrodes, including bare GCE, HLCNT/GCE, HLCNT-AuNPs-1/GCE and HLCNT-AuNPs-2/GCE, were measured in a 5 mM $[Fe(CN)_6]^{3-/4-}$ solution, where the redox peak currents were 127.69, 221.26, 202.50, and 232.75 μA, respectively. We found that the GCE was the smallest peak. Compared to GCE, HLCNT/GCE showed a larger redox peak in solution because HLCNT has good conductivity.

Among these electrodes, HLCNT-AuNPs-2/GCE showed the largest anode and cathode peak currents, due to $[Fe(CN)_6]^{3-/4-}$ having the fastest electrical-transfer rate on HCNT-AuNPs-2/GCE. According to the Randles–Sevcik equation,[26] the calculation of the electroactive surface area (ESA) of the different electrodes can be performed by:

$$I_p = 2.69 \times 10^5 \, AD^{1/2} n^{3/2} \gamma^{1/2} c$$

where I_p is the peak current (A), n is the number of electrons transferred, A is the ESA (cm^2) of the electrode, D is the diffusion coefficient of the molecule in the $[Fe(CN)_6]^{3-/4-}$ solution (cm^2 s^{-1}), c is the volume concentration of the probe (mol cm^{-3}) and γ is the scanning rate (V s^{-1}). The diffusion coefficient (D) probe of $[Fe(CN)_6]^{3-/4-}$ was $(6.70 \pm 0.02) \times 10^{-6}$ cm^2 s^{-1}. The concentration of the $[Fe(CN)_6]^{3-/4-}$ redox couple was 5 mM. The ESA values of GCE, HLCNT/GCE, HLCNT-AuNPs-1/GCE and HLCNT-AuNPs-2/GCE were 0.1160, 0.1838, 0.2009 and 0.2113 cm^2, respectively. Combining the good conductivity of HLCNT and the conductance of AuNPs, HLCNT-AuNPs-2 accelerated the transfer speed of electrons.

EIS is an effective method to estimate electron transfer, which is closely related to the electrochemical properties of the HLCNT. The Nyquist plot consisted of a semicircle following the line. The semicircle is related to the charge-transfer process, and the line region corresponds to the reverse control process. The Nyquist plots of the bare GCE, HLCNT/GCE, HLCNT-AuNPs-1/GCE, HLCNT-DA/GCE, HLCNT-DA-AuNPs/GCE, HLCNT-AuNPs-2/GCE, HLCNT-AuNPs-2-D-Tyr/GCE and HLCNT-AuNPs-2-L-Tyr/GCE in buffer solution containing 5 mM $[Fe(CN)_6]^{3-/4-}$ are shown in Fig. 5B. As can be seen from the figure, GCE was the electrode with the highest impedance among these electrodes, which was 280 Ω, indicating that its electron-transfer rate was the slowest. The impedance of HLCNT/GCE was 2.6 Ω, which showed that HLCNT greatly promoted the electron transfer of the electrode. After adding DA, the impedance value of HLCNT-DA/GCE was 49.83 Ω, which was increased compared with HLCNT/GCE, indicating that DA and HLCNT interacted well. The impedance of HLCNT-DA-AuNPs/GCE was 205.4861 Ω, indicating that the AuNPs were loaded on HLCNT-DA/GCE. For HLCNT-AuNPs-1/GCE, the R_{ct} was increased to 68.72 Ω, indicating that the AuNPs were loaded on the HLCNT/GCE. The R_{ct} of HLCNT-AuNPs-2/GCE was 48.802 Ω, which indicated that the addition of KOH to remove DA was beneficial to the dispersion of the AuNPs. The HLCNT-AuNPs-2-D-Tyr/GCE impedance value was 67.507 Ω. After combining D-Tyr, the R_{ct} increased, which was caused by the spatial effect of HLCNT-AuNPs-2 and D-Tyr. For HLCNT-AuNPs-2-L-Tyr/GCE, the impedance value was 94.331 Ω, indicating that D-Tyr had a faster electron-transfer rate than L-Tyr on HLCNT-AuNPs-2.

Electrochemical recognition of Tyr enantiomers

The electrochemical behaviour of 0.75 mM Tyr enantiomer on the GCE, HLCNT/GCE, HLCNT-AuNPs-1/GCE, HLCNT-AuNPs-2/GCE was detected by DPV in 0.1 M PBS solution (pH = 7.4). From Fig. 6, the peak potentials of D-Tyr and L-Tyr were shown to be 0.93 V (line a) and 0.93 V (line b) on the GCE, and ΔE_p was 0 mV, explaining that the glassy carbon electrode could not recognize the amino acid isomers. However, ΔE_p on HLCNT/GCE was 0.02 V (lines c and d), showing that HLCNT enabled the chiral recognition of Tyr. The ΔE_p on HLCNT-AuNPs-1/GCE was 0.012 V (lines e and f), which may indicate the effect of the spatial structure of HLCNT and the combination with AuNPs. Also, for HLCNT-AuNPs-2/GCE, the value was 0.024 V (lines g and h), showing that after the PDA was polymerized, the AuNPs were more uniformly dispersed on the surface, which enhanced the synergistic effect and the chiral recognition performance of

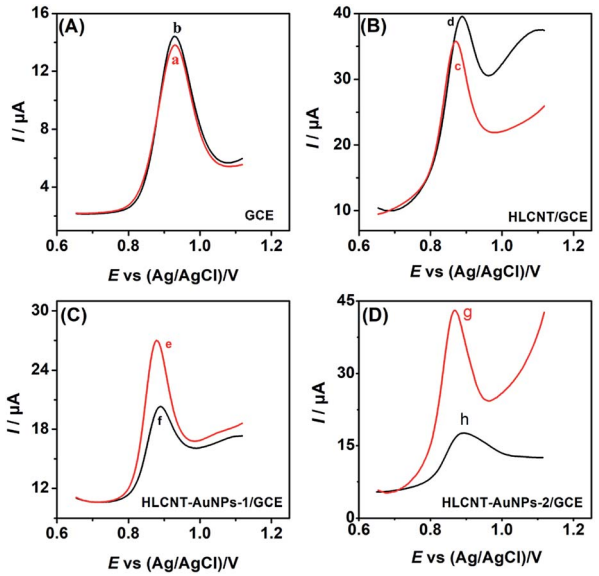

Fig. 6 (A) DPVs of D-Tyr (a) and L-Tyr (b) on GCE; (B) DPVs of D-Tyr (c) and L-Tyr (d) on HLCNT/GCE; (C) DPVs of D-Tyr (e) and L-Tyr (f) on HLCNT-AuNPs-1/GCE; (D) DPVs of D-Tyr (g) and L-Tyr (h) on HLCNT-AuNPs-2/GCE. L-Tyr and D-Tyr concentration: 0.75 mM; pulse amplitude: 0.05 V, pulse width: 0.05 s, pulse period: 0.5 s.

the AuNPs and HLCNT. From these data, it can be concluded that HLCNT-AuNPs-2 had a better chiral recognition ability than the others, and this can ascribed to the synergistic effect of HLCNT with the chiral structure and the highly dispersed AuNPs.[23] The difference between HLCNT-AuNPs-2/GCE with L/D-Tyr and L/D-Trp is that such attachment may result in a difference in the free energy, which then causes a possible change in the electrochemical detection signal.[14,29] Among these, in HLCNT-AuNPs-2/GCE, the current response of D-Tyr is much greater than L-Tyr. This result indicates that HLCNT-AuNPs-2/GCE with a distinctive left-handed double helix chiral structure may bond with D-Tyr more stably than L-Tyr, and the above behavior brings a lower free energy.[27]

Therefore, we chose HLCNT-AuNPs-2 with the Tyr enantiomer with the largest ΔI_p and ΔE_p as the best material for the next experiments.

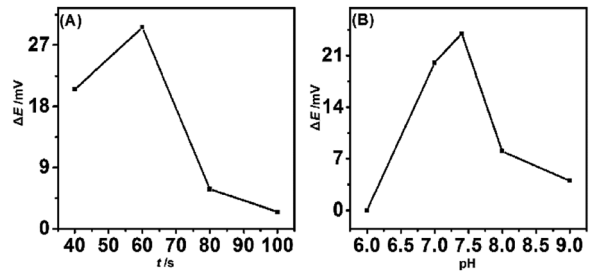

Fig. 7 (A) The different ΔE_p of 0.75 mM L-Tyr, D-Tyr on HLCNT-AuNPs-2/GCE with different loading times of AuNPs; (B) the different ΔE_p of 0.75 mM L-Tyr, D-Tyr on HLCNT-AuNPs-2 with different pHs.

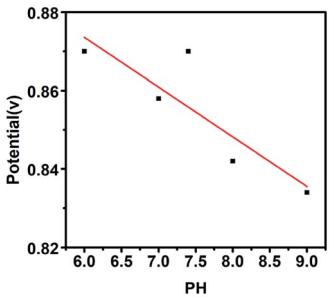

Fig. 8 The variation of potential *versus* pH for D-Tyr on HLCNT-AuNPs-2/GCE.

Impact of Au loading time

To achieve higher recognition efficiency, the effect of gold loading for the chiral discrimination was studied. From Fig. 7A, it can be seen that from 40 s to 60 s, the ΔE_P of L-Tyr and D-Tyr gradually increased but then dropped sharply after 60 s. When t was 60 s, the ΔE_P of L-Tyr and D-Tyr on HLCNT-AuNPs-2/GCE was 0.0295 V, suggesting that the interaction of HLCNT-AuNPs-2 and Tyr enantiomers had reached saturation. Based on the potential difference results, we optimized the load time and used 60 s as load time to measure L-Tyr and D-Tyr.

Effect of pH

The effects of L-Tyr and D-Tyr electrooxidation on the HLCNT-AuNPs-2/GCE at different pH values in 0.1 M PBS buffer solution were investigated in Fig. 7B. As can be seen from the (ΔE_P)-pH diagram, the ΔE_P of L-Tyr and D-Tyr gradually increased from pH 6.0 to pH 7.4, but then decreased sharply after pH 7.4. The buffer solution plays a very important role in the enantiospecific action.[28] When the pH is near neutral, the interaction between HLCNT-AuNPs-2 and D-Tyr was stronger than at other pH values. Therefore, L-Tyr and D-Tyr were measured using a buffer solution of pH = 7.4. Furthermore, it can be clearly seen in Fig. 8 that as the pH value increased, the oxidation peak potentials of D-Tyr on HLCNT-AuNPs-2/GCE were negatively shifted, indicating that protons were directly involved in the electrochemical oxidation process.[29] Simultaneously, as can be seen from the regression equations for the potential and pH (Fig. 8), the slope value was 13 mV/pH, indicating the existence of proton electron transfer in the electrochemical process.

Application of Tyr chiral recognition in the racemic solution

Based on our optimized experimental conditions, the prepared HLCNT-AuNPs-2/GCE was used to detect the electrochemical chirality in the Tyr racemic solution based on the potential and current difference signal. Fig. 9A illustrates the DPVs of different L-Tyr% (10%, 20%, 30%, 40%, 50%, 60%, 70%) of a 0.75 mM Tyr racemic mixture on HLCNT-AuNPs-2/GCE, and Fig. 9B shows the linear relationship between I (a red dot), E (b black dot) and different L-Tyr%, where the equation is E (V) = $0.874 + 6.42 \times 10^{-4}$ L-Tyr%, I (μA) = 21.92–0.19 L-Tyr% and the linear range was 0.075 mM L-Tyr to 0.525 mM L-Tyr. It can be seen that as L-Tyr% increases, the peak potential positively

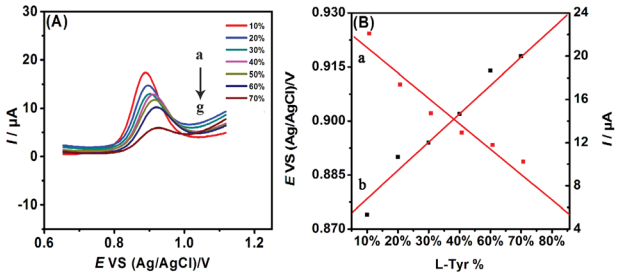

Fig. 9 (A) DPVs of different L-Tyr% of a 0.75 mM Tyr racemic mixture on HLCNT-AuNPs-2/GCE in 0.1 M PBS solution (pH = 7.4). L-Tyr percentage (a to g, %): 10%, 20%, 30%, 40%, 50%, 60%, 70%; (B) relationship between *I* ((a) red dot), *E* ((b) black dot) and different L-Tyr%.

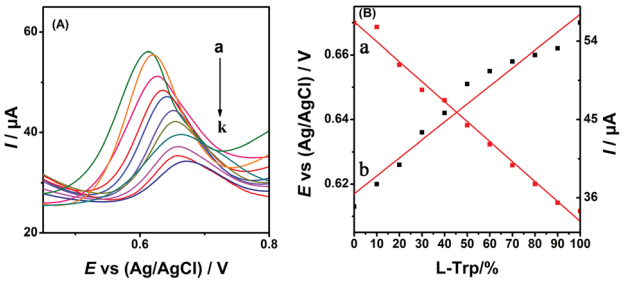

Fig. 11 (A) DPVs of different L-Trp% of a 0.5 mM Trp racemic mixture on HLCNT-AuNPs-2/GCE in 0.1 M PBS solution (pH = 7.4), L-Trp percentage (a to k, %): 0%, 10%, 20%, 30%, 40%, 50%, 60%, 70%, 80%, 90%, 100%; (B) relationship between *I* ((a) red dot), *E* ((b) black dot) and different L-Trp%.

shifts and the peak current decreases, and the lower detection limit was 9.04 μM for L-Tyr. That is, HLCNT-AuNPs-2/GCE could quantitatively detect L-Tyr in the racemic solution of Tyr and the D-Tyr enantiomer based on the potential and current. Differences in HLCNT-AuNPs-2/GCE and L/D-Tyr attachment may result in differences in the free energy, reflecting potential changes in the electrochemical measurements.[28] Due to the special space structure of HLCNT-AuNPs-2, it has a stronger attachment to D-Tyr than L-Tyr and has a lower free energy; therefore, as L-Tyr% increases, the potential increases and the current reduces.

Electrochemical recognition of Trp enantiomers

We further investigated the electrochemical behaviour of 0.5 mM Trp enantiomers on GCE, HLCNT/GCE, HLCNT-AuNPs-1/GCE, HLCNT-AuNPs-2/GCE by the DPV method in 0.1 M PBS solution (pH = 7.4). In Fig. 10, we can clearly see a trend in ΔI_p and ΔE_p from Fig. 10A to 10B. The ΔE_p values on GCE, HLCNT/GCE, HLCNT-AuNPs-1/GCE and HLCNT-AuNPs-2/GCE were 0.007 V (lines a and b), 0.008 V (lines c and d), 0.023 V (lines e and f) and 0.062 V (lines g and h). From the results, we can see that HLCNT-AuNPs-2 had better chiral recognition ability than the others. Therefore, we chose HLCNT-AuNPs-2 with the Trp enantiomer of the largest ΔI_p and ΔE_p as the best material in the experiment. The detected D-Trp potential was slightly to the left than the L-Trp potential, and the current was higher than L-Trp, which also showed the ability of the HLCNT-AuNPs-2 material to better bind and recognize D-Trp.

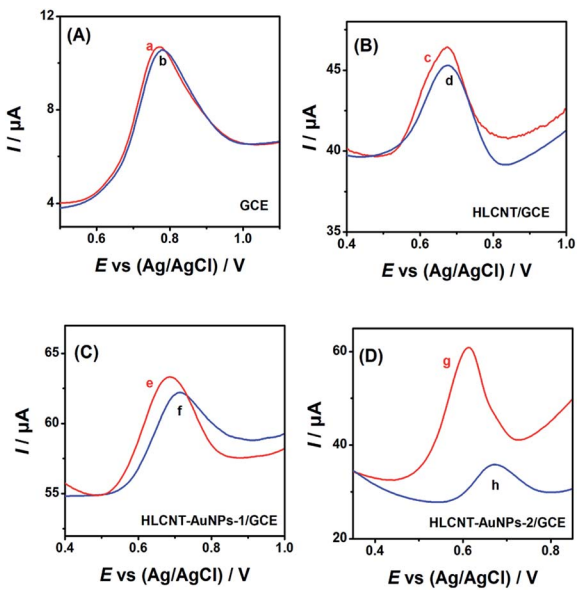

Fig. 10 (A) DPVs of D-Trp (a) and L-Trp (b) on GCE; (B) DPVs of D-Trp (c) and L-Trp (d) on HLCNT/GCE; (C) DPVs of D-Trp (e) and L-Trp (f) on HLCNT-AuNPs-1/GCE; (D) DPVs of D-Trp (g) and L-Trp (h) on HLCNT-AuNPs-2/GCE. L-Trp and D-Trp concentration: 0.5 mM; pulse amplitude: 0.05 V, pulse width: 0.05 s, pulse period: 0.5 s.

Application of Trp chiral recognition in the racemic solution

Based on the above, we also selected the prepared HLCNT-AuNPs-2/GCE to detect the electrochemical chirality in the Trp racemic solution based on the potential difference in the signal. Fig. 11A illustrates the DPVs of different L-Trp% (a–k: 0%, 10%, 20%, 30%, 40%, 50%, 60%, 70%, 80%, 90%, 100%) of a 0.5 mM Trp racemic mixture on HLCNT-AuNPs-2/GCE, and Fig. 11B exhibits the good linear relationship between *I* ((a) red dot), *E* ((b) black dot) and different L-Trp%, where the equation is E (V) = 0.617 + 5.56 × 10^{-4} L-Trp%, I (μA) = 56.25–0.23 L-Trp% and the linear range was 0.05 mM L-Trp to 0.5 mM L-Trp. It can be seen that as L-Trp% increases, the peak potential is positively shifted and the peak current decreases, and the detection limit was calculated to be 5.31 μM for L-Trp. Furthermore, a comparison of the developed sensor with previously reported chiral sensors is given in Table 1. That is, HLCNT-AuNPs-2/GCE could quantitatively detect L-Trp in the racemic solution of Trp and the D-Tyr enantiomer based on the potential and current. Differences in HLCNT-AuNPs-2/GCE and L/D-Trp attachment may result in differences in free energy. As a result of the space structure of HLCNT-AuNPs-2, it has stronger attachment to D-Trp than L-Trp, leading to a lower free energy; so, as L-Trp% increases, the current reduces and the potential increases.

Determination of L-tyrosine in real samples

To demonstrate the application potential, the HLCNT-AuNPs-2/GCE was used to analyze L-tyrosine tablets. An L-tyrosine sample

Table 1 Comparison of the developed sensors for the recognition of Tyr enantiomers and Trp enantiomers

Electrode	Method	Linear range (mM)	Limit of detection (μM)	Ref.
MWCNTs-EA-NCCS/GCE	CV	1–10	—	1
rGO/γ-CD/GCE	DPV	0.1–1	21(L-Trp)	30
PCDP/MWCNT/GCE	DPV	0.008–2	—	31
β-CD-PtNPs/GNs/GCE	DPV	0.05–5	17(L-Trp)	32
β-CDs-GQDs	DPV	—	10.3(D-Tyr)	33
PLC/MWCNTs/GCE	DPV	0.1–1	33(L-Tyr)	2
HLCNT-AuNPs-2	DVP	0.05–0.5, 0.075–0.525	5.31(L-Trp), 9.04(L-Tyr)	This work

Table 2 Determination of L-tyrosine in an L-tyrosine tablet sample

Sample	Labelled[a] (mg mL^{-1})	Added (mg mL^{-1})	Found (mg mL^{-1})	Recovery (%)
1	0.03255	0.03255	0.03226	99.13
2	0.03255	0.06510	0.06690	102.77
3	0.03255	0.09765	0.09809	100.45

[a] The sample was diluted 40 times with pH 7.4 PBS.

was prepared by dissolving L-tyrosine caplets (containing 500 mg of L-tyrosine) in 384 mL of formic acid solution (1 : 1). The detection was carried out by the standard addition method, and the results are shown in Table 2. It can be seen that the experiment has a good recovery rate, which proved that HLCNT-AuNPs-2/GCE could be used to detect the content of L-tyrosine in real samples.

Conclusions

In this work, a typical HLCNT/AuNPs composite was successfully prepared *via* adding AuNPs on the surface of HLCNT by an electrochemical method and this was used as a chiral electrocatalyst for Tyr and Trp enantiomer recognition. Here, the loaded dopamine acted as a locating agent to make the AuNPs disperse uniformly on the carbon nanotubes. HLCNT-AuNPs-2 combined the conductivity of AuNPs with the chiral structure of carbon nanotubes, so that under the optimized experimental parameters the electrochemical determination of L/D-Tyr and L/D-Trp in their mixed solution could be successfully achieved in the detection. Based on the different oxidation potentials and current signals, the HLCNT-AuNPs-2/GCE exhibited a lower detection limit and a higher sensitivity. It achieves the qualitative and quantitative detection of Tyr and Trp enantiomers. Moreover, this work built a novel potential-based electrochemical chiral biosensing system based on the chiral carbon nanotubes that demonstrated excellent performance when used for the detection of actual samples of amino acids. This work is of great importance in real chiral biosensing research, which can be further applied in biosensors.

Conflicts of interest

There are no conflicts to declare.

Acknowledgements

This work was supported by the Natural Science Foundation of Hebei Province (No. B2018201214, No. B2019201407), the Chunhui Program of Ministry of Education of China, the Priority Strategy Project of Key Laboratory of Medicinal Chemistry and Molecular Diagnosis of Ministry of Education (ts2019003).

Notes and references

1 Z. L. Li, Z. L. Mo, P. J. Yan, S. J. Meng, R. J. Wang, X. H. Niu, N. J. Liu and R. B. Guo, Chiral electrochemical recognition of tryptophan enantiomers at a multi-walled carbon nanotube-N-carboxymethyl chitosan composite modified glassy carbon electrode, *New J. Chem.*, 2018, **42**, 11635–11641.
2 D. M. Guo, Y. H. Huang, C. Chen, Y. Chen and Y. Z. Fu, A sensing interface for recognition of tryptophan enantiomers based on porous cluster-like nanocomposite films, *New J. Chem.*, 2014, **38**, 5880–5885.
3 W. M. Xuan, M. N. Zhang, Y. Liu, Z. J. Chen and Y. Cui, A chiral quadruple-stranded helicate cage for enantioselective recognition and separation, *J. Am. Chem. Soc.*, 2012, **134**, 6904–6907.
4 M. Z. H. Khan, X. Liu, Y. Tang, *et al.*, A glassy carbon electrode modified with a composite consisting of gold nanoparticle, reduced graphene oxide and poly(L-arginine) for simultaneous voltammetric determination of dopamine, serotonin and L-tryptophan, *Microchim. Acta*, 2018, **185**, 439.
5 C. N. Beuning, B. Mestre-Voegtlé, P. Faller, C. Hureau and D. C. Crans, Measurement of interpeptidic Cu (II) exchange rate constants by static fluorescence quenching of tryptophan, *Inorg. Chem.*, 2018, **57**, 4791–4794.
6 J. A. Kwon, C. M. Jin, Y. Shin, H. Y. Kim, Y. Kim, T. Kang and I. Choi, Tunable plasmonic cavity for label-free detection of small molecules, *ACS Appl. Mater. Interfaces*, 2018, **10**, 13226–13235.
7 S. Szunerits, Y. Coffinier, E. Galopin, J. Brenner and R. Boukherroub, Preparation of boron-doped diamond nanowires and their application for sensitive electrochemical detection of tryptophan, *Electrochem. Commun.*, 2010, **12**, 438–441.
8 M. Govindasamy, V. Mani, S. Chen, *et al.*, Methyl parathion detection in vegetables and fruits using silver@ graphene

nanoribbons nanocomposite modified screen printed electrode, *Sci. Rep.*, 2017, **7**, 46471.

9 A. B. Hashkavayi and J. B. Raoof, Ultrasensitive and reusable electrochemical aptasensor for detection of tryptophan using of [Fe(bpy)3](p-CH3C6H4SO2)2 as an electroactive indicator, *J. Pharm. Biomed. Anal.*, 2019, **163**, 180–187.

10 F. Biedermann and W. M. Nau, Noncovalent chirality sensing ensembles for thedetection and reaction monitoring of amino acids peptides, proteins, and aromatic drugs, *Angew. Chem., Int. Ed.*, 2014, **53**, 5694–5699.

11 Y. Tao, F. Chu, X. Gu, Y. Kong, Y. Lv and L. Deng, A novel electrochemical chiral sensor for tyrosine isomers based on a coordination-driven self-assembly, *Sens. Actuators, B*, 2018, **255**, 255–261.

12 L. Challier, F. Mavré, J. Moreau, *et al.*, *Anal. Chem.*, 2012, **84**, 5415.

13 Y. Haldorai, A. T. E. Vilian, M. Rethinasabapathy, Y. S. Huh and Y. Han, Electrochemical determination of dopamine using a glassy carbon electrode modified with TiN-reduced graphene oxide nanocomposite, *Sens. Actuators, B*, 2017, **247**, 61–69.

14 X. Zeng, N. Li and J. C. Wang, Electrochemical synthesis of (poly) dimethoxyaniline on glassy carbon electrodes and their applications in the detection of L- and D-glutamic acids, *J. Electrochem. Soc.*, 2019, **166**, B3066–B3071.

15 Q. J. Kingsford, D. P. Zhang, Y. Z. Ma, *et al.*, Electrochemically Recognizing Tryptophan Enantiomers based on Carbon Black/Poly-l-Cysteine Modified Electrode, *J. Electrochem. Soc.*, 2019, **166**, B1226–B1231.

16 M. V. Kharlamova, C. Kramberger, Y. Sato, *et al.*, Chiral vector and metal catalyst-dependent growth kinetics of singlewall carbon nanotubes, *Carbon*, 2018, **133**, 283–292.

17 J. T. Wang, X. Jin, Z. B. Liu, G. Yu, *et al.*, Growing highly pure semiconducting carbon nanotubes by electrotwisting the helicity, *Nat. Catal.*, 2018, **1**, 326–331.

18 S. H. Liu, Y. Y. Duan, X. J. Feng, J. Yang and S. N. Che, Synthesis of enantiopure carbonaceous nanotubes with optical activity, *Angew. Chem., Int. Ed.*, 2013, **52**, 6858–6862.

19 J. W. Gao, M. M. Chen, W. Wen, *et al.*, Au-Luminol-decorated porous carbon nanospheres for the electrochemiluminescence biosensing of MUC1, *Nanoscale*, 2019, **11**, 16860–16867.

20 S. H. Chen, Y. X. Wang, M. X. Zhong, *et al.*, Fe(III)-Tannic Acid Complex Derived Fe3C Decorated Carbon Nanofibers for Triple-Enzyme Mimetic Activity and Their Biosensing Application, *ACS Biomater. Sci. Eng.*, 2019, **5**, 1238–1246.

21 M. E. Lynge, R. Westen, A. Postma and B. Stadler, Polydopamine—a nature-inspired polymer coating for biomedical science, *Nanoscale*, 2011, **3**, 4916–4928.

22 D. Q. Zhang, M. C. Wen, S. S. Zhang, P. J. Liu, W. Zhu, G. S. Li and H. X. Li, Au nanoparticles enhanced rutile TiO2 nanorod bundles with high visible-light photocatalytic performance for NO oxidation, *Appl. Catal., B*, 2014, **147**, 610–616.

23 Y. Chen, Z. X. Fan, Z. M. Luo, X. Z. Liu, Z. C. Lai, B. Li, Y. Zong, L. Gu and H. Zhang, High Yield synthesis of crystal-phase-heterostructured 4H/fcc Au@Pd core–shell nanorods for electrocatalytic ethanol oxidation, *Adv. Mater.*, 2017, **19**, 1701331.

24 L. Wu, F. Li, Y. Y. Xu, J. W. Zhang, D. Q. Zhang, G. S. Li and H. X. Li, Plasmon-induced photoelectrocatalytic activity of Au nanoparticles enhanced TiO2 nanotube arrays electrodes for environmental remediation, *Appl. Catal., B*, 2015, **164**, 217–224.

25 Y. T. Yu, H. B. Qiu, X. W. Wu, *et al.*, Synthesis and characterization of silica nanotubes with radially oriented mesopores, *Adv. Funct. Mater.*, 2008, **18**, 541–550.

26 L. Y. Ma, L. J. Bai, M. Zhao, *et al.*, An electrochemical aptasensor for highly sensitive detection of zearalenone based on PEI-MoS2-MWCNTs nanocomposite for signal enhancement, *Anal. Chim. Acta*, 2019, **1060**, 71–78.

27 A. Berthod, Chiral recognition mechanisms, *Anal. Chem.*, 2006, **78**, 2093–2099.

28 F. Scholz and R. Gulaboski, Gibbs energies of transfer of chiral anions across the interface water chiral organic solvent determined with the help of three-phase electrodes, *Faraday Discuss.*, 2005, **129**, 169–177.

29 J. Zou and J. G. Yu, Nafion-stabilized black phosphorus nanosheets-maltosyl-β-cyclodextrin as a chiral sensor for tryptophan enantiomers, *Mater. Sci. Eng. C*, 2020, **112**, 110910.

30 E. Zor, E. Morales-Narvaez, S. Alpaydin, H. Bingol, M. Ersoz and A. Merkoci, Graphene-based hybrid for enantioselective sensing applications, *Biosens. Bioelectron.*, 2017, **87**, 410–416.

31 X. Liu, S. Zhang, H. Xu, Y. Zhang, L. Dong, S. Gao, L. Zhong and T. Jiang, Enhanced electrochemical enantiorecognition of tryptophan enantiomers based on synergistic effect of porous β-CD-containing polymers and multiwalled carbon nanotubes, *Microchem. J.*, 2020, **155**, 104688.

32 J. J. Xu, Q. H. Wang, C. Z. Xuan, Q. Xia, X. Lin and Y. Z. Fu, Chiral recognition of tryptophan enantiomers based on b-cyclodextrin-platinum nanoparticles/graphene nanohybrids modified electrode, *Electroanalysis*, 2016, **28**, 868–873.

33 S. Dong, Q. Bi, C. Qiao, Y. Sun, X. Zhang, X. Lu and L. Zhao, Electrochemical sensorfor discrimination tyrosine enantiomers using graphene quantum dots and beta-cyclodextrins composites, *Talanta*, 2017, **173**, 94–100.

